Cavity quantum electrodynamics for a cylinder: Inside a hollow dielectric and near a solid dielectric cylinder

H. Nha and W. Jhe
Department of Physics, Seoul National University, Seoul 151-742, Korea
(Received 6 August 1996; revised manuscript received 21 March 1997)

We calculate the atomic energy-level shift and the modified dipolar radiation rate inside a hollow dielectric cylinder and outside a solid cylinder using a quantum-mechanical linear-response formalism in the dipole approximation. We first derive the electromagnetic fields scattered by the cylindrical surface for an oscillating dipole inside and outside the cylinder. When an atom is located on the axis of the cylindrical hollow, we obtain analytic expressions of the atomic level shifts in two limiting cases: when b (radius of hollow) is very small, the level shift is proportional to b^{-2} which is associated with the kinetic-energy change of the atomic electron, whereas when b is very large, the shift is proportional to b^{-4} which is identified as the retarded (Casimir-Polder) interaction energy. Moreover, we calculate the atomic potentials as a function of the position of atoms in the hollow region, which is important for the atom-guiding experiment. We also calculate the decay rates and find enhanced rates inside and outside the cylinder. In particular, we compare the radiative properties of an atom inside the hollow cylinder with those between two plates, and those near a cylinder with near a single surface. [S1050-2947(97)03608-1]

PACS number(s): 42.50.Ct, 32.70.Jz, 12.20.Ds

I. INTRODUCTION

There has been much interest and activity devoted to the study of cavity quantum electrodynamics (cavity QED) [1] for various cavity geometries. For example, there are numerous theoretical or experimental studies of atomic energy-level shifts and modified radiative decay rates near a single surface [2,3], between parallel surfaces [4–6], and inside or outside of a spherical cavity [7,8]. Recently, the cavity QED effects inside a hollow dielectric cylinder or near a solid dielectric cylinder have also become interesting and attractive, in particular, in the fields of atom optics and atomic spectroscopy in a microcavity.

For instance, an atomic waveguide with blue-detuned evanescent waves in an hollow optical fiber was suggested by Marksteiner *et al.* [9] and it has been recently realized by Renn *et al.* [10] and by Ito *et al.* [11]. In particular, isotope separation as well as the observation of cavity QED effects was achieved in Ref. [11]. Atoms were also guided by a red-detuned Gaussian laser in the hollow region [12]. A similar, small hollow fiber may be used to study the quantum statistical properties of atoms in one dimension [13] or even to realize atomic quantum wire [14]. It has been also suggested that a stable, helical motion of an atom around a solid optical fiber may be possible by using evanescent waves developed near the cylindrical surface [14]. Moreover, a quantum nondemolition measurement of the photon number inside an optical fiber was performed using the Compton scattering of the electrons due to the evanescent waves produced near the fiber [15].

Despite its increasing interest and importance, no theoretical work has been done for a cylindrical cavity (inside or outside), except for a classical study of the damping-rate change and frequency shift of the cyclotron motion of a free electron inside a cylindrical microwave cavity [16]. Therefore, it seems urgently necessary to study the cavity-QED effects for the cylindrical geometry in detail. (We should especially know the attractive potential by the cylindrical surface for the analysis of the experiments related to guiding inside the fiber.) Note that the results of Ref. [16] are not appropriate since they only deal with the classical electronic motion inside a perfectly conducting cavity. We therefore need a more general quantum-mechanical treatment, including the effects of dielectric material as well as polarizations of the atomic dipole.

Although a general approach to the problem may be the perturbation theory with quantized cavity fields, it is not useful since it becomes very complicated and almost impossible for problems other than the perfect-conductor case of simple geometries. In this paper, on the other hand, we will use the linear-response formalism [4] which has been successfully applied to other geometries [5,7]. We will calculate the dispersive and dissipative cavity-QED effects inside as well as outside a dielectric cylinder. In Sec. II, we solve the scattering problem inside and outside the cylinder to obtain the electric fields reflected by the cylindrical surfaces. We then obtain the field susceptibilities and calculate the level shifts, as well as the modified decay rates, inside a hollow dielectrtic cylinder in Sec. III and the decay rates outside a conducting cylinder in Sec. IV, where the results are compared to those for other geometries. In Sec. V we obtain the level shifts as a function of atomic position inside the hollow dielectric and outside the cylindrical dielectric. Conclusions and comments are made in Sec. VI.

II. RADIATION FIELDS SCATTERED BY CYLINDRICAL SURFACES

A. Inside a hollow dielectric

In this subsection, we calculate the scattered fields due to the cylindrical surface when the atomic dipole is located in-

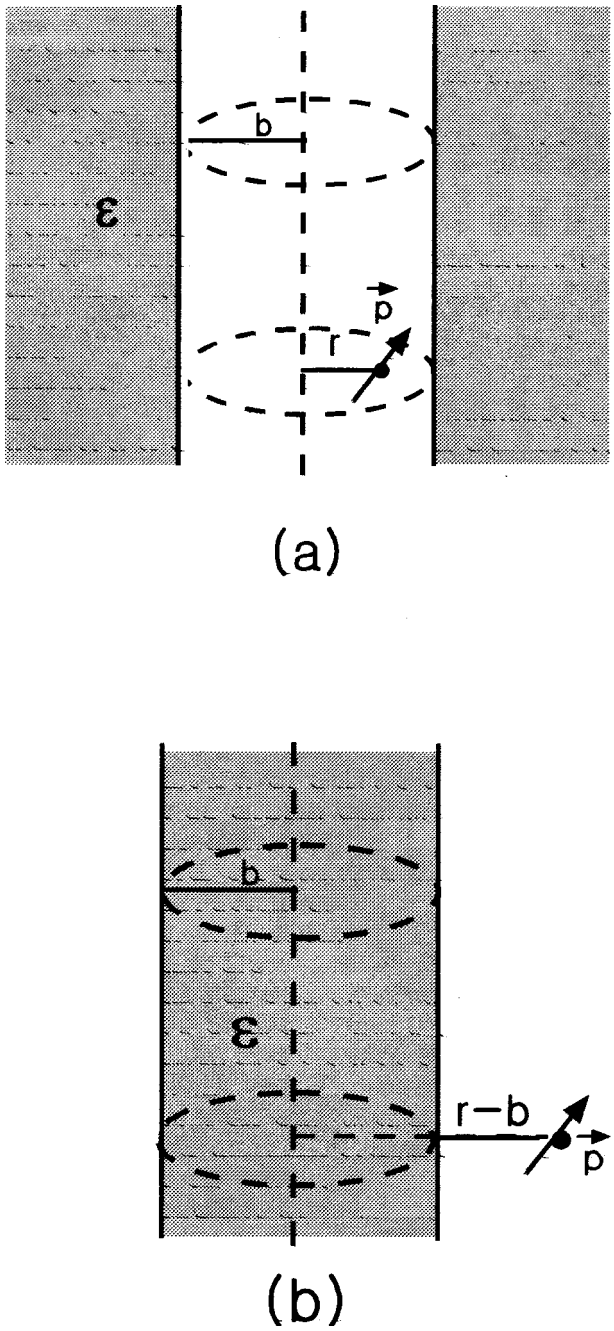

FIG. 1. (a) Geometry for the scattering problem when the dipole is inside a hollow dielectric cylinder radius b and (b) when the atom is outside a solid cylinder. The cylinder radius is b and the dielectric constant is ϵ.

side a cylindrical cavity made up of a long, hollow dielectric [see Fig. 1(a)]. In free space, the dipole fields are obtained from the vector potential $\vec{A}$

$$\vec{A}=-ik\vec{p}\frac{e^{ik|\vec{r}-\vec{r}_0|}}{|\vec{r}-\vec{r}_0|},$$

$$\vec{B}=\vec{\nabla}\times\vec{A},$$

$$\vec{E}=\frac{i}{k}\vec{\nabla}\times\vec{B}, \tag{2.1}$$

where $\vec{B}$ ($\vec{E}$) is the magnetic (electric) field, $\omega(=ck)$ is the oscillation frequency, and $\vec{r}_0$ is the dipole location.

By the eigenfuction expansion (refer to Appendix A for its derivation), we find

$$\frac{e^{ik|\vec{r}-\vec{r}_0|}}{|\vec{r}-\vec{r}_0|}=\frac{i}{2}\sum_{m=-\infty}^{\infty}\int_{-\infty}^{\infty}dk' e^{im(\phi-\phi')}e^{ik'(z-z')} \times J_m(\sqrt{k^2-k'^2}\rho_<)H_m^{(1)}(\sqrt{k^2-k'^2}\rho_>), \tag{2.2}$$

where $\rho_<$ ($\rho_>$) is the smaller (larger) of ρ and ρ_0 and $J_m(x)$ [$H_m^{(1)}(x)$] is the Bessel function [Hankel function] of the first kind.

Then, from Eqs. (2.1) and (2.2), we obtain the free fields in terms of the cylindrical eigenfunctions. When the dipole is located inside a hollow cylinder surrounded by the dielectric surface (dielectric constant ϵ), the scattered fields along the axis (i.e., z components) are found as

$$E_z^{sc}=\sum_{m=-\infty}^{\infty}\int_{-\infty}^{\infty}dk' J_m(\alpha_1\rho)e^{im\phi}e^{ik'z}a_{mk'}, \tag{2.3}$$

$$H_z^{sc}=\sum_{m=-\infty}^{\infty}\int_{-\infty}^{\infty}dk' J_m(\alpha_1\rho)e^{im\phi}e^{ik'z}b_{mk'}, \tag{2.4}$$

and the transmitted fields are obtained as

$$E_z^{t}=\sum_{m=-\infty}^{\infty}\int_{-\infty}^{\infty}dk' H_m(\alpha_2\rho)e^{im\phi}e^{ik'z}c_{mk'}, \tag{2.5}$$

$$H_z^{t}=\sum_{m=-\infty}^{\infty}\int_{-\infty}^{\infty}dk' H_m(\alpha_2\rho)e^{im\phi}e^{ik'z}d_{mk'}, \tag{2.6}$$

where $\alpha_1=\sqrt{k^2-k'^2}$ and $\alpha_2=\sqrt{\epsilon k^2-k'^2}$. [For simplicity, we write $H_m^{(1)}(x)$ as $H_m(x)$.] Moreover, ρ and ϕ components of the fields can be calculated from the z components by Maxwell's equations. Therefore, we only have to determine the coefficients $a_{mk'}$, $b_{mk'}$, $c_{mk'}$, and $d_{mk'}$ using the standard boundary conditions.

From the continuities of the ϕ and z components of E and H fields, we obtain

$$e^z_{mk'}+J_m(\alpha_1 b)a_{mk'}=H_m(\alpha_2 b)c_{mk'},$$

$$h^z_{mk'}+J_m(\alpha_1 b)b_{mk'}=H_m(\alpha_2 b)d_{mk'},$$

$$\frac{im}{b}J_m(\alpha_1 b)a_{mk'}-\frac{\alpha_1\omega}{k'c}J'_m(\alpha_1)b_{mk'}-i\frac{\alpha_1^2}{k'}e^{\phi}_{mk'} =\frac{\alpha_1^2}{\alpha_2^2}\left(\frac{im}{b}H_m(\alpha_2 b)c_{mk'}-\frac{\alpha_2\omega}{k'c}H'_m(\alpha_2 b)d_{mk'}\right),$$

$$\frac{im}{b}J_m(\alpha_1 b)b_{mk'}+\frac{\alpha_1\omega}{k'c}J'_m(\alpha_1)a_{mk'}-i\frac{\alpha_1^2}{k'}h^{\phi}_{mk'}$$

$$= \frac{\alpha_1^2}{\alpha_2^2}\left(\frac{im}{b} H_m(\alpha_2 b) d_{mk'} + \frac{\epsilon \alpha_2 \omega}{k' c} H'_m(\alpha_2 b) c_{mk'} \right), \tag{2.7}$$

where

$$e^z_{mk'} = \frac{i}{2}\Big[\alpha_1^2 J_m(\alpha_1\rho_0) H_m(\alpha_1 b) p_3 - k'\alpha_1 J_{m-1}(\alpha_1\rho_0) H_m(\alpha_1 b) \frac{ip_1+p_2}{2} + k'\alpha_1 J_{m+1}(\alpha_1\rho_0) H_m(\alpha_1 b) \frac{ip_1-p_2}{2} \Big],$$

$$e^\phi_{mk'} = \frac{i}{2}\Big[-\frac{mk'}{b} J_m(\alpha_1\rho_0) H_m(\alpha_1 b) p_3 + J_{m-1}(\alpha_1\rho_0) \times \left(k^2 H_{m-1}(\alpha_1 b) - \frac{m\alpha_1}{b} H_m(\alpha_1 b) \right) \frac{ip_1+p_2}{2} + J_{m+1}(\alpha_1\rho_0) \left(k^2 H_{m+1}(\alpha_1 b) - \frac{m\alpha_1}{b} H_m(\alpha_1 b) \right) \frac{-ip_1+p_2}{2} \Big],$$

$$h^z_{mk'} = -\frac{ik}{4} \alpha_1 H_m(\alpha_1 b) [J_{m-1}(\alpha_1\rho_0)(p_1 - ip_2) + J_{m+1}(\alpha_1\rho_0)(p_1 + ip_2)],$$

$$h^\phi_{mk'} = \frac{ik}{2}\Big[k' J_{m-1}(\alpha_1\rho_0) H_{m-1}(\alpha_1 b) \frac{p_1 - ip_2}{2} + k' J_{m+1}(\alpha_1\rho_0) H_{m+1}(\alpha_1 b) \frac{p_1 + ip_2}{2} + i\alpha_1 J_m(\alpha_1\rho_0) H'_m(\alpha_1 b) p_3 \Big]. \tag{2.8}$$

Here p_1, p_2, and p_3 represent p_x, p_y, and p_z, respectively, and J'_m and H'_m stand for the derivatives of J_m and H_m. For convenience, we have assumed without loss of generality that the dipole position is such that $\phi_0 = z_0 = 0$. Using Eqs. (2.6) and (2.7), we now can calculate the coefficients $a_{mk'}$ to $d_{mk'}$.

For instance, when the dipole is inside a perfectly conducting cylinder ($\epsilon \to \infty$),

$$a_{mk'} = -\frac{e^z_{mk'}}{J_m(\alpha_1 b)},$$

$$b_{mk'} = -i \frac{k'}{k\alpha_1 J'_m(\alpha_1 b)} \left(\frac{m}{b} e^z_{mk'} + \frac{\alpha_1^2}{k'} e^\phi_{mk'} \right),$$

$$c_{mk'} = d_{mk'} = 0. \tag{2.9}$$

Note that in dealing with the coefficients, we need careful treatments so that the scattered fields do not diverge: we first replace $k = \omega/c$ by $k(1 + i\epsilon)$ and then set $\epsilon \to 0_+$ (this procedure is also related to causality).

B. Outside a solid dielectric

In Sec. II A, we have solved the scattering problem when the dipole is inside a hollow dielectric cylinder. On the other hand, the above results can be simply applied to the case where the dipole is outside a solid dielectric cylinder. In this case, $\rho_<$ ($\rho_>$) becomes b (ρ_0) at the boundary $\rho = b$ and we need to exchange $J_m(x)$ and $H_m(x)$ in all the equations of Sec. II in order for the scattered and transmitted fields not to diverge.

III. ATOMIC DECAY RATE AND LEVEL SHIFT INSIDE A HOLLOW DIELECTRIC CYLINDER

In this section, using the results of the preceding section and the linear-response theory [2], we first obtain the field susceptibilities as

$$G_{\alpha\beta} = G^0_{\alpha\beta} + G^R_{\alpha\beta}, \tag{3.1}$$

where $G^0_{\alpha\beta}$ is the free-space susceptibility in the absence of the cavity and $G^R_{\alpha\beta}$ is the susceptibility for the field reflected by the cylindrical surfaces [5]. We then calculate the modified decay rate and the energy-level shift of an atom by

$$\frac{\Gamma_{fi}}{\Gamma^0_{fi}} = 1 + \frac{2}{\hbar\Gamma^0_{fi}} p^{fi}_\alpha p^{if}_\beta \mathrm{Im} G^R_{\alpha\beta}(\vec{r}_0, \vec{r}_0; \omega_0), \tag{3.2}$$

and

$$\delta E = -\frac{\hbar}{2\pi} \int_0^\infty d\zeta \; G^R_{\alpha\beta}(\vec{r}_0, \vec{r}_0; i\zeta) \alpha_{\alpha\beta}(i\zeta), \tag{3.3}$$

respectively. Here p^{fi}_α is the α component of the matrix element of the atomic dipole operator $\vec{p}$ between two atomic states $|i\rangle$ and $|f\rangle$, $\hbar\omega_0$ is the corresponding energy-level difference, Γ^0_{fi} is the free-space decay rate, and $\alpha_{\alpha\beta}(\omega)$ is the atomic susceptibility (refer to Ref. [5] for details).

A. σ-polarization case

Let us first consider the σ-polarization case where the radiative dipole is polarized along the cylinder axis (that is, $p_1 = p_2 = 0$). Therefore, we only need E^{sc}_z at the atom position. From Eq. (2.3), we find

$$G^R_\sigma = \sum_{m=-\infty}^{\infty} \int_{-\infty}^{\infty} dk' J_m(\alpha_1\rho') a'_{mk'}, \tag{3.4}$$

where ρ' is the distance between the atom and the cylinder axis and $a'_{mk'} = a_{mk'}/p_3$ since $p_1 = p_2 = 0$.

Then, using Eqs. (3.2)–(3.4), we can obtain the modified radiative decay rate and the ground-state energy-level shift. In particular, when the atom is on the axis [that is, $\rho' = 0$ in Fig. 1(a)], only $m = 0$ term survives so that we find, in case of σ polarization,

$$\frac{\Gamma_\sigma}{\Gamma_0} = \frac{3}{2} \mathrm{Re} \int_0^\infty dx \; \alpha_1^2 \alpha_2 \frac{H_0(\alpha_2\xi)}{J_0(\alpha_1\xi)} A, \tag{3.5}$$

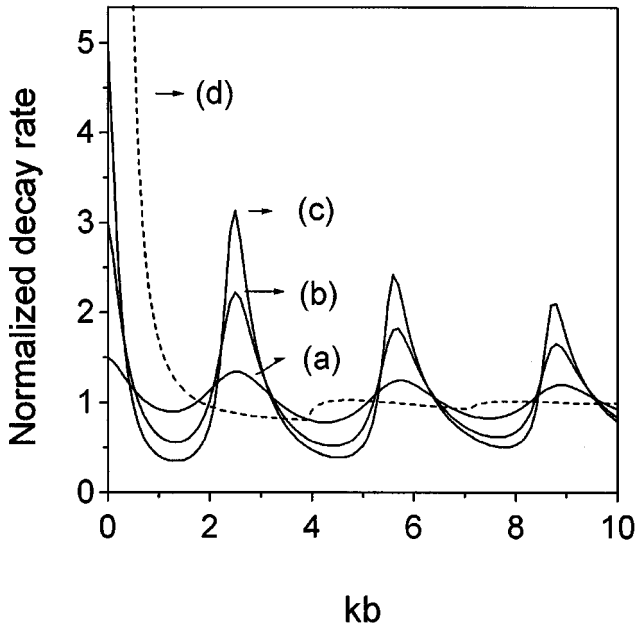

FIG. 2. Modified decay rate normalized to the free-space value as a function of $kb=2\pi b/\lambda$, when the atom is on the axis of the hollow cylinder, for σ polarization with (a) $\epsilon=2.25$, (b) $\epsilon=9$, (c) $\epsilon=25$, and for (d) π polarization inside a conducting cylinder.

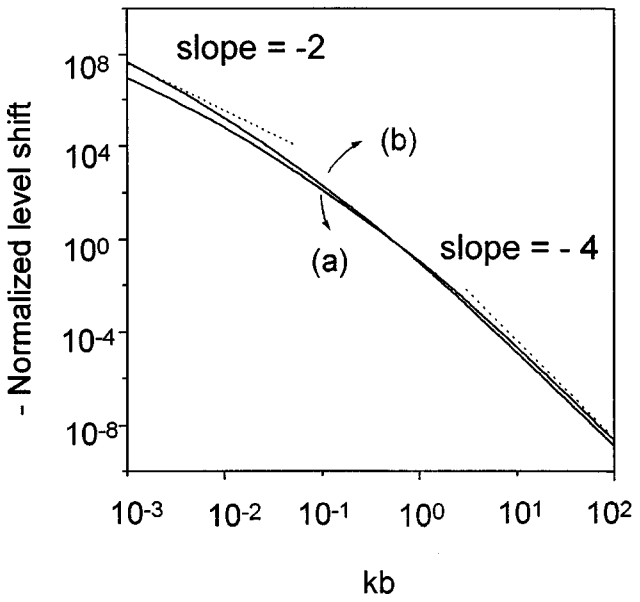

FIG. 3. Energy-level shift of the ground-state atom (in log scale) normalized to $\hbar\Gamma_0$ as a function of $kb=2\pi b/\lambda$, when the atom is on the axis of a conducting cylinder, for (a) σ and (b) π polarization.

$$\delta E_0^{\sigma}=-\frac{2}{\pi^2}\sum_n\left(\frac{\omega_{n0}}{c}\right)^3|p_z^{0n}|^2\int_0^{\infty}\int_0^{\infty}dx\,dy\frac{\alpha^2y^3}{1+y^2}B, \tag{3.6}$$

where

$$A(\epsilon,\alpha_1,\alpha_2,\xi)=\frac{J_1(\alpha_1\xi)H_0(\alpha_1\xi)-J_0(\alpha_1\xi)H_1(\alpha_1\xi)}{\alpha_2J_1(\alpha_1\xi)H_0(\alpha_2\xi)-\epsilon\alpha_1J_0(\alpha_1\xi)H_1(\alpha_2\xi)}, \tag{3.7}$$

$$B(\epsilon,\alpha,\beta,x,y,z)=\frac{\epsilon\alpha K_1(\beta yz)K_0(\alpha yz)-\beta K_1(\alpha yz)K_0(\beta yz)}{\epsilon\alpha K_1(\beta yz)I_0(\alpha yz)+\beta I_1(\alpha yz)K_0(\beta yz)}, \tag{3.8}$$

and

$$\alpha_1=\sqrt{1-x^2},\quad \alpha_2=\sqrt{\epsilon-x^2},\quad \xi=kb=2\pi b/\lambda,$$

$$\alpha=\sqrt{1+x^2},\quad \beta=\sqrt{\epsilon+x^2},\quad z=\omega_{n0}b/c.$$

Here Γ_0 simply denotes Γ_{fi}^0 and $K_m(x),I_m(x)$ are the modified Bessel functions.

In Fig. 2, we plot the decay rates as a function of the normalized distance $\xi=2\pi b/\lambda$ where b is the radius of the cylinder and λ is the transition wavelength. Figures 2(a)–2(c) present the modified decay rates when the atom is on the cylinder axis for $\epsilon=2.25,9,25$, respectively. As shown in the figures, we observe that when ξ is near $x_{0n}=2.41,5.52,8.65$, etc., where x_{mn} is the nth root of $J_m(x_{mn})=0$, the decay rate is larger than the free-space value and the enhancement factor increases as the dielectric constant ϵ increases. (Note that new propagating TM modes appear at $\xi=x_{0n}$). The general behavior of the decay rate with respect to the cylinder radius is similar to that of the case of an atom at the midpoint of the parallel dielectric plates [5], whereas the oscillatory trend is more pronounced in the cylinder case even in the large ξ region: the approach of the normalized decay rate to unity (or, the free-space value) is slower than that for the two plate case. The cavity effects are, therefore, rather significant even for a large radius of the cylinder. From Fig. 2, we can also find how the decay rate changes with ϵ. For example, in the case of large dielectric constant, strong inhibition of spontaneous emission is expected when ξ is not very close to x_{0n}.

Next, let us consider the level shift. Using Eqs. (3.6) and (3.8), one can evaluate the energy shifts numerically. On the other hand, one can also easily obtain the analytical expressions of the shifts in the short-range and long-range limits, that is, for $b\to 0$ and $b\to\infty$, respectively.

For small $z=\omega_{n0}b/c$ (or short-range limit), we obtain

$$\delta E_0^{\sigma}=-\frac{2}{\pi^2}\frac{I_{1\epsilon}^{\sigma}}{b^2}\sum_n\left(\frac{\omega_{n0}}{c}\right)|p_z^{0n}|^2=-\frac{\hbar e^2I_{1\epsilon}^{\sigma}}{mc\pi^2b^2}, \tag{3.9}$$

where

$$I_{1\epsilon}^{\sigma}=\int_0^{\infty}\int_0^{\infty}dx\,dy\,\alpha^2y\times\frac{\epsilon\alpha K_1(\beta y)K_0(\alpha y)-\beta K_1(\alpha y)K_0(\beta y)}{\epsilon\alpha K_1(\beta y)I_0(\alpha y)+\beta I_1(\alpha y)K_0(\beta y)}, \tag{3.10}$$

with $\alpha=\sqrt{1+x^2}$ and $\beta=\sqrt{\epsilon+x^2}$. In the derivation of Eq. (3.9), we have used the Thomas-Reiche-Kuhn sum rule and $I_{1\epsilon}^{\sigma}$ is a numerical constant depending on the dielectric constant ϵ.

As can be seen in Eq. (3.9), the level shift in the short-range limit shows b^{-2} dependence (also refer to Fig. 3) but

the usual van der Waals interaction (b^{-3}) is not observed when the atom is on the cylinder axis. This result is different from that of the two plate case but very similar to that of a spherical cavity: when the atom is at the center of a spherical cavity, the short-range interaction also shows b^{-2} behavior with a different coefficient [7]. Equations (3.9) and (3.10) also indicate that the short-range shift has no dependence on the atomic internal states. The physical implication of this interaction energy is discussed in the following paragraphs.

In the Coulomb gauge, the interaction Hamiltonian can be written as

$$H_I = -\frac{e}{mc}\vec{P}\cdot\vec{A} + \frac{e^2}{2mc^2}\vec{A}^2, \tag{3.11}$$

where $\vec{P}$ is the atomic momentum operator. When we calculate the energy shift to order e^2 in the perturbation theory, the second term of Eq. (3.11) produces the state-independent shift. Moreover, this A^2 interaction describes the kinetic energy associated with the vibration of the atomic electron in the fluctuating electromagnetic field [17–20]. Therefore we can observe that Eq. (3.10) represents the renormalized kinetic energy of the electron wobbled by vacuum fluctuation inside a hollow cylindrical cavity.

For large z (or the long-range limit), on the other hand, we obtain

$$\delta E_0^{\sigma} = -\frac{2}{\pi^2}\frac{I_{2\epsilon}^{\sigma}}{b^4}\sum_n \left(\frac{c}{\omega_{n0}}\right)|p_z^{0n}|^2 = -\frac{\hbar c I_{2\epsilon}^{\sigma}\alpha_z(0)}{\pi^2 b^4}, \tag{3.12}$$

where

$$I_{2\epsilon}^{\sigma} = \int_0^{\infty}\int_0^{\infty} dx\ dy\ \alpha^2 y^3 \times \frac{\epsilon\alpha K_1(\beta y)K_0(\alpha y) - \beta K_1(\alpha y)K_0(\beta y)}{\epsilon\alpha K_1(\beta y)I_0(\alpha y) + \beta I_1(\alpha y)K_0(\beta y)} \tag{3.13}$$

and $\alpha_z(0)$ is the static atomic polarizability given by

$$\alpha_z(0) = \sum_n \frac{2|p_z^{0n}|^2}{\hbar\omega_{n0}}. \tag{3.14}$$

Equation (3.12) is the well-known Casimir-Polder retardation energy having b^{-4} dependence (see also Fig. 3). Note that both short-range and long-range interaction energy, which is proportional to $\hbar$, are associated with pure quantum-mechanical effects.

To obtain the full-range behavior, we assume an oscillator atom, that is, we consider only $n=1$ term which corresponds to a strongly coupled, first-excited state. In Fig. 3(a), the level shift, normalized to $\hbar\Gamma_0$, is shown as a function of $kb = 2\pi b/\lambda$ when the atom is on the axis of a perfectly conducting hollow cylinder (i.e., $\epsilon\to\infty$). As is clear, one can explicitly distinguish the short-range and the long-range limit. For a dielectric cavity, on the other hand, the general behaviors are similar to those of the conductor case, but only the absolute values are different. We therefore need to know, for a detailed evaluation, only the numerical constants $I_{1\epsilon}^{\sigma}$ and $I_{2\epsilon}^{\sigma}$ for each value of ϵ. For example, when $\epsilon = 2.25$, $I_1^{\sigma}\approx 40.37$, and $I_2^{\sigma}\approx 0.95$.

B. π-polarization case

When the atomic dipole is polarized perpendicular to the cylinder axis (π polarization such that $p_3 = 0$), we can proceed by the same method as in the σ-polarization case. In Fig. 2(d), we have plotted the normalized decay rate when the atom is on the axis of a perfectly conducting hollow cylinder. In this case, the behavior is very similar to that for the parallel-plate case [5]. Moreover, the behavior in case of a dielectric cavity is also similar to that of the conductor case except the fact that the decay rate is finite at $\xi = kb = 0$.

For the level shift, we obtain in the short-range limit

$$\delta E_0^{\pi} = -\frac{2}{\pi^2}\frac{I_{1\epsilon}^{\pi}}{b^2}\sum_n \left(\frac{\omega_{n0}}{c}\right)|p_{\perp}^{0n}|^2 = -\frac{\hbar e^2 I_{1\epsilon}^{\pi}}{mc\pi^2 b^2}, \tag{3.15}$$

and in the long-range limit

$$\delta E_0^{\pi} = -\frac{2}{\pi^2}\frac{I_{2\epsilon}^{\pi}}{b^4}\sum_n \left(\frac{c}{\omega_{n0}}\right)|p_{\perp}^{0n}|^2 = -\frac{\hbar c I_{2\epsilon}^{\pi}\alpha_{\perp}(0)}{\pi^2 b^4}, \tag{3.16}$$

where

$$I_{1\epsilon}^{\pi} = \int_0^{\infty}\int_0^{\infty} dx\ dy \frac{n(\epsilon,x,y)}{d(\epsilon,x,y)}, \tag{3.17}$$

$$I_{2\epsilon}^{\pi} = \int_0^{\infty}\int_0^{\infty} dx\ dy\ y^2 \frac{n(\epsilon,x,y)}{d(\epsilon,x,y)}, \tag{3.18}$$

and

$$d(\epsilon,x,y) = I_1^2\left(1-\frac{\alpha^2}{\beta^2}\right)^2 + \alpha^2\frac{y^2}{x^2}\left(I_1' - \frac{\alpha K_1'}{\beta K_1}I_1\right) \times \left(I_1' - \epsilon\frac{\alpha K_1'}{\beta K_1}I_1\right),$$

$$n(\epsilon,x,y) = \frac{y^2\alpha^2}{\beta}\left(\frac{\alpha}{\beta}I_1' - \frac{K_1'}{K_1}I_1\right)K_0' - y^3\alpha^2 K_0\left(I_1' - \frac{\alpha K_1'}{\beta K_1}I_1\right) + y^3\alpha^2 K_0'\left[\epsilon\left(\frac{\alpha}{\beta}I_1' - \frac{\alpha^2 k_1'}{\beta^2 K_1}I_1\right)\frac{K_1'}{K_1} + \frac{x^2}{y^2\beta^2} \times \left(1-\frac{\alpha^2}{\beta^2}\right)I_1\right] - y\alpha\left(1-\frac{\alpha^2}{\beta^2}\right)I_1(yK_0 + \alpha K_0'). \tag{3.19}$$

Note that in Eq. (3.19), the argument of the modified Bessel functions I_1, K_0 and their derivatives I_1', K_0', is αy, whereas that of K_1 and K_1' is βy.

The physical implications of the interaction energy in the short-range and the long-range limit are identical to those of the σ-polarization case. In Fig. 3(b), we present the numerical result and we find that the long-range level shifts are

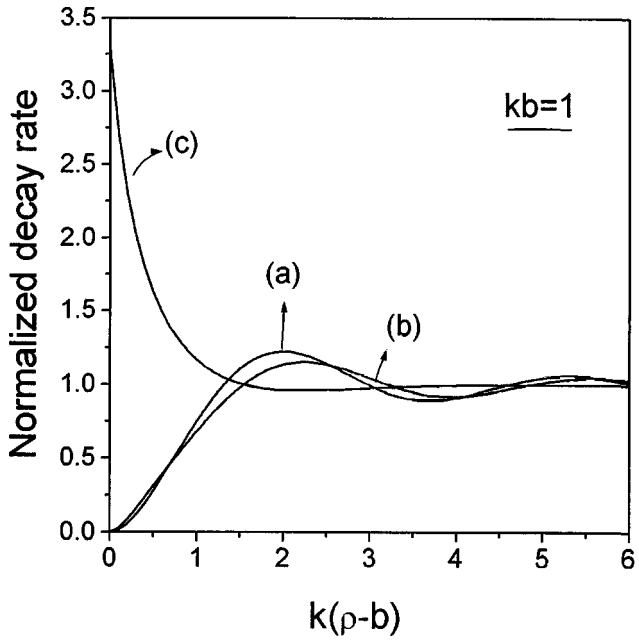

FIG. 4. Modified decay rate as a function of the normalized distance $k(\rho-b)$, when the atom is outside a conducting cylinder and $kb=1$, for (a) σ_z, (b) σ_ϕ, and (c) π polarization.

nearly the same for two polarizations, however, the short-range shift for π polarization is slightly larger than that for σ polarization. One can also consider other interesting problems, such as the level shifts as a function of the atom's position for a given hollow radius. We will discuss this issue in Sec. V.

IV. DECAY RATE NEAR A SOLID CYLINDER

In this section, for simplicity, we present the modified decay rate when an atom is outside a conducting cylinder. With simple modifications, as mentiond in Sec. II B, the equations become very similar to those derived in Sec. IV and consequently we just plot the numerical results without presenting the formulas here. When the atom is near a solid cylinder, three different atomic polarizations are possible [see Fig. 1(b)]: a dipole parallel to the cylinder axis (σ_z polarization), perpendicular to the axis but tangential to the surface (σ_ϕ polarization), and perpendicular to the axis but normal to the surface (π polarization).

In Fig. 4, we have presented the decay rates for the three polarizations as a function of the normalized distance from the surface $k(\rho-b)=2\pi(\rho-b)/\lambda$ for a given b such that $kb=2\pi b/\lambda=1$, where ρ is the atom-axis separation. The variations of the σ_z polarization and the σ_ϕ polarization are nearly the same with each other. Moreover, we find that the general behaviors for the three cases are similar to that for a single plane-surface case. In the case of the single plate, however, the decay rate for a dipole normal to the surface is enhanced by a factor of 2 when the dipole-surface separation approaches zero. As can be seen from Fig. 4, on the other hand, the enhancement factor is more than 3 when $kb=1$. This larger enhancement can be attributed to the finite radius of the curvature of the cylindrical surface and we have checked that the plane-surface result can be recovered when the radius becomes very large. We consequently conclude that the enhancement effect is more significant when the atom is near a cylindrical surface rather than near a plane surface.

V. LEVEL SHIFT AS A FUNCTION OF ATOMIC POSITION

In this section, we present the level shifts of the ground state as a function of the radial position for fixed radius b inside the hollow fiber and outside the solid dielectric fiber. They are very useful for experiments such as atom guidance, for which one should know the atomic potential in addition to the optical potential. When the atom is inside the hollow region and at an off-axis position, we have three different polarizations, as in the case outside the fiber (Sec. V). For σ_z polarization, the shift is

$$\delta E_0^{\sigma_z}=-\frac{1}{\pi}\Sigma_n\int_0^\infty d\xi\frac{\omega_{n0}|p_z^{0n}|^2}{\omega_{n0}^2+\xi^2}G_{zz}(r,r,i\xi), \tag{5.1}$$

where

$$G_{zz}(r,r,\omega)=\frac{i}{2}\Sigma_m\int dk'\,\alpha_1^2[J_m(\alpha_1 r)]^2 \times H_m(\alpha_1 b)\frac{PU_z+QV_z}{P^2+QR} \tag{5.2}$$

and r is the atomic distance from the center ($k=\omega/c$). [For the expressions of P, Q, R, U_i, and $V_i(i=\rho,\phi,z)$ which depend on b, m, k, k', and ϵ, see Appendix B.]

For σ_ϕ and π polarization, on the other hand, the shifts are

$$\delta E_0=-\frac{1}{\pi}\Sigma_n\int_0^\infty d\xi\frac{\omega_{n0}|p_i^{0n}|^2}{\omega_{n0}^2+\xi^2}G_{ii}(r,r,i\xi), \tag{5.3}$$

where $i=\rho,\phi$ and

$$G_{\rho\rho}(r,r,\omega)=i\Sigma_m\int dk'\,\frac{k'}{\alpha_1^2}\left(\alpha_1 J_m'(\alpha_1 r)\frac{PU_\rho+QV_\rho}{P^2+QR}+\frac{imk}{k'}J_m(\alpha_1 r)\frac{PV_\rho-RU_\rho}{P^2+QR}\right), \tag{5.4}$$

$$G_{\phi\phi}(r,r,\omega)=i\Sigma_m\int dk'\,\frac{k'}{\alpha_1^2}\left(\frac{im}{r}J_m(\alpha_1 r)\frac{PU_\phi+QV_\phi}{P^2+QR}-\frac{\alpha_1 k}{k'}J_m'(\alpha_1 r)\frac{PV_\phi-RU_\phi}{P^2+QR}\right). \tag{5.5}$$

Using the above results, we can calculate the atomic level shifts for various atomic positions. For example, in Fig. 5, we present the level shift of a two-level atom (σ_z polarization) normalized to $\hbar\Gamma$ when the atom is inside the hollow dielectric ($\epsilon=2.25$) with $kb=2\pi b/\lambda=5$ with the normalized distance $r/b<1$. We observe the short-range van der Waals type potential near the surface. Moreover, this range becomes even smaller as kb increases. When the atom is outside the cylindrical dielctric, on the other hand, we only

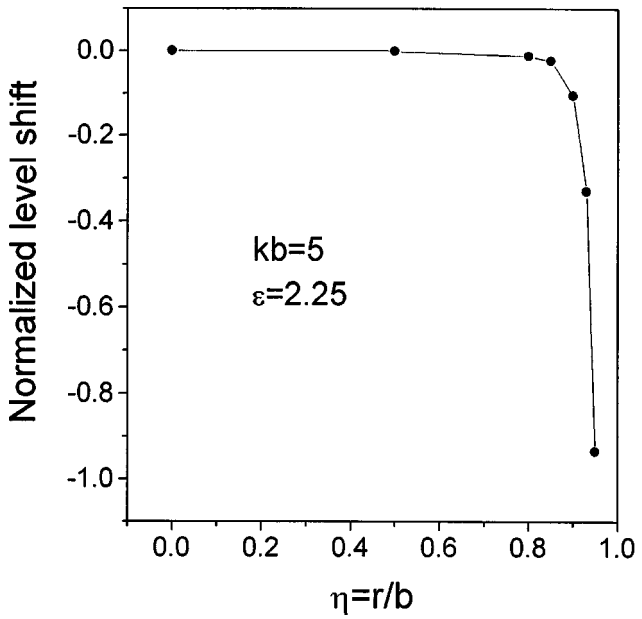

FIG. 5. Energy-level shift of the ground-state atom normalized to $\hbar\Gamma_0$ is presented as a function of $\eta=r/b$, when the σ_z-polarized atom is inside the dielectric hollow region.

have to exchange $J_m(x)$ with $H_m(x)$ (and vice versa) in all the equations. Note that $r/b>1$ in this case.

VI. CONCLUSIONS

In summary, we have calculated the decay rates and the level shifts of an atom when it is inside a hollow dielectric cylinder, and the decay rate when the atom is ouside a solid dielectric cylinder. In particular, we have obtained the analytical expressions in two limiting cases. When the atom is on the axis of the hollow cylinder, the short-range level shift scales as b^{-2}, whereas the long-range shift goes as b^{-4}. Each energy shift is attributed to the state-independent interaction due to vacuum fluctuation and the Casimir-Polder retarded interaction, respectively. We have also compared the decay rates inside the hollow cylinder to those between parallel plates, and the results outside a solid cylinder to those near a plane surface. The similarities, as well as the differences, are discussed in detail. Moreover, we obtained the level shift as a function of atomic radial distance for fixed radius inside the dielectric hollow and outside the cylindrical dielectric.

The general equations and specific results presented in this paper may be useful for some experiments in quantum optics and atom optics. For example, the results for a hollow optical fiber may be applied to a realization of atomic quantum wire [14], laser cooling and trapping in the hollow [13], and cavity-QED effects therein [11]. The results for a solid optical fiber may be also applied to the atomic helical motion guided along the fiber's outer surface by a blue-detuned laser coupled into the fiber core [14]. Experimental studies of these possibilities are under investigation.

ACKNOWLEDGMENTS

We are grateful to the Ministry of Education (BSRI 96-2421), the Ministry of Science and Technology of Korea, and the Korean Atomic Energy Research Institute for financial support.

APPENDIX A: DERIVATION OF EQ. (2.2)

First, we note that $G(\vec{r},\vec{r}')=e^{ik|\vec{r}-\vec{r}'|}/(4\pi|\vec{r}-\vec{r}'|)$ is the radially outgoing solution of the equation

$$(\nabla^2+k^2)G(\vec{r},\vec{r}\,')=-\delta(\vec{r},\vec{r}')=-\frac{1}{\rho}\delta(\rho-\rho')\times\delta(\phi-\phi')\delta(z-z'). \tag{A1}$$

Since

$$\delta(\phi-\phi')=\frac{1}{2\pi}\sum_{m=-\infty}^{\infty}e^{im(\phi-\phi')},$$

and

$$\delta(z-z')=\frac{1}{2\pi}\int_{-\infty}^{\infty}e^{ik'(z-z')}, \tag{A2}$$

we can write $G(\vec{r},\vec{r}')$ as

$$G(\vec{r},\vec{r}')=\frac{1}{4\pi^2}\sum_{m=-\infty}^{\infty}\int_{-\infty}^{\infty}dk'e^{im(\phi-\phi')}\times e^{ik'(z-z')}g_m(k',\rho,\rho'). \tag{A3}$$

To determine $g_m(k',\rho,\rho')$, we insert Eq. (A3) into Eq. (A1) and obtain

$$\left[\frac{1}{\rho}\frac{d}{d\rho}\left(\rho\frac{d}{d\rho}\right)+\left(k^2-k'^2-\frac{m^2}{\rho^2}\right)\right]g_m=-\frac{1}{\rho}\delta(\rho-\rho'). \tag{A4}$$

Due to the finiteness at the origin and the radially outgoing property, we assume the appropriate solution as

$$g_m(k',\rho,\rho')=AJ_m(k\rho_<)H_m^{(1)}(k\rho_>), \tag{A5}$$

where $\rho_<(\rho_>)$ is the smaller (larger) of ρ and ρ'. The constant A can be determined by the discontinuity in the slope due to the δ function in Eq. (A4)

$$\left.\frac{dg_m}{d\rho}\right|_+-\left.\frac{dg_m}{d\rho}\right|_-=-\frac{1}{\rho'}. \tag{A6}$$

Since $W(J_m(x),H_m^{(1)}(x))=2i/\pi x$ where W denotes the Wronskian, we obtain $A=\pi i/2$. Consequently, we obtain

$$\frac{e^{ik|\vec{r}-\vec{r}'|}}{|\vec{r}-\vec{r}'|}=\frac{i}{2}\sum_{m=-\infty}^{\infty}\int_{-\infty}^{\infty}dk'e^{im(\phi-\phi')}e^{ik'(z-z')}J_m\times(\sqrt{k^2-k'^2}\rho_<)H_m^{(1)}(\sqrt{k^2-k'^2}\rho_>). \tag{A7}$$

APPENDIX B: FORMULAS IN SEC. VI

In this Appendix, $\alpha_1=\sqrt{k^2-k'^2}$, $\alpha_2=\sqrt{\epsilon k^2-k'^2}$, and the argument of the Bessel function $J_m(H_m)$ and its derivative

$J'_m(H'_m)$ is $\alpha_1 b$ $(\alpha_2 b)$ unless it is explicitly specified. Then the functions are given as

$$P=\frac{im}{b}\left(1-\frac{\alpha_1^2}{\alpha_2^2}\right)J_m, \tag{B1}$$

$$Q=\frac{\alpha_1 k}{k'}J'_m-\frac{k\alpha_1^2}{\alpha_2 k'}\frac{H'_m}{H_m}J_m, \tag{B2}$$

$$R=\frac{\alpha_1 k}{k'}J'_m-\frac{\epsilon k\alpha_1^2}{\alpha_2 k'}\frac{H'_m}{H_m}J_m, \tag{B3}$$

$$U_z=-\frac{im}{b}\left(1-\frac{\alpha_1^2}{\alpha_2^2}\right), \quad V_z=\frac{\epsilon\alpha_1^2 k}{\alpha_2 k'}-\frac{\alpha_1 k}{k'}\frac{H'_m}{H_m}. \tag{B4}$$

And for U_ρ, U_ϕ, V_ρ, and V_ϕ, we have

$$U_i=\frac{i\alpha_1^2}{k'}f_i^\phi+\frac{im\alpha_1^2}{b\alpha_2^2}f_i^z-\frac{k\alpha_1^2}{k'\alpha_2}\frac{H'_m}{H_m}g_i^z, \tag{B5}$$

$$V_i=\frac{i\alpha_1^2}{k'}g_i^\phi+\frac{im\alpha_1^2}{b\alpha_2^2}g_i^z+\frac{\epsilon k\alpha_1^2}{k'\alpha_2}\frac{H'_m}{H_m}f_i^z \quad (i=\rho,\phi), \tag{B6}$$

where

$$f_\rho^z=-ik'\alpha_1 J'_m(\alpha_1 r)H_m(\alpha_1 b),$$

$$g_\rho^z=-\frac{ikm}{2r}J_m(\alpha_1 r)H_m(\alpha_1 b), \tag{B7}$$

$$f_\rho^\phi=\Big[k^2(J_{m+1}(\alpha_1 r)H_{m+1}(\alpha_1 b)-J_{m-1}(\alpha_1 r)H_{m-1}(\alpha_1 b))+\frac{2m\alpha_1}{b}J'_m(\alpha_1 r)H_m(\alpha_1 b)\Big]\Big/4, \tag{B8}$$

$$g_\rho^\phi=ikk'(J_{m-1}(\alpha_1 r)H_{m-1}(\alpha_1 b)+J_{m+1}(\alpha_1 r)H_{m+1}(\alpha_1 b))/4, \tag{B9}$$

and

$$f_\phi^z=-mk'\alpha_1 J_m(\alpha_1 r)H_m(\alpha_1 b)/r,$$

$$g_\phi^z=-k\alpha_1 J'_m(\alpha_1 r)H_m(\alpha_1 b)/2, \tag{B10}$$

$$f_\phi^\phi=i\Big[k^2(J_{m+1}(\alpha_1 r)H_{m+1}(\alpha_1 b)+J_{m-1}(\alpha_1 r)H_{m-1}(\alpha_1 b))-\frac{2m^2\alpha_1}{b}J_m(\alpha_1 r)H_m(\alpha_1 b)\Big]\Big/4, \tag{B11}$$

$$g_\phi^\phi=kk'(J_{m-1}(\alpha_1 r)H_{m-1}(\alpha_1 b)-J_{m+1}(\alpha_1 r)H_{m+1}(\alpha_1 b))/4. \tag{B12}$$

[1] See, for example, *Cavity Quantum Electrodynamics*, edited by P. R. Berman (Academic, New York, 1994).
[2] J. M. Wylie and J. E. Sipe, Phys. Rev. A **30**, 1185 (1984).
[3] D. Meschede, W. Jhe, and E. A. Hinds, Phys. Rev. A **41**, 1587 (1990).
[4] G. Barton, Proc. R. Soc. London, Ser. A **320**, 251 (1970); **410**, 141 (1987); W. Jhe, Phys. Rev. A **43**, 5795 (1991); **44**, 5932 (1991).
[5] H. Nha and W. Jhe, Phys. Rev. A **54**, 3505 (1996).
[6] J.-Y. Courtois, J.-M. Courty, and J. C. Mertz, Phys. Rev. A **53**, 1862 (1996).
[7] W. Jhe and K. Jang, Phys. Rev. A **53**, 1126 (1996).
[8] V. V. Klimov, M. Ducloy, and V. S. Letokhov, J. Mod. Opt. **43**, 549 (1996).
[9] S. Marksteiner, C. M. Savage, P. Zoller, and S. L. Rolston, Phys. Rev. A **50**, 2680 (1994).
[10] M. J. Renn, E. A. Donley, E. A. Cornell, C. E. Wieman, and Z. Anderson, Phys. Rev. A **53**, R648 (1996).
[11] H. Ito, T. Nakada, K. Sakaki, M. Ohtsu, K. I. Lee, and W. Jhe, Phys. Rev. Lett. **76**, 4500 (1996).
[12] M. J. Renn, E. Montgomery, O. Vdovin, D. Z. Anderson, C. E. Wieman, and E. A. Cornell, Phys. Rev. Lett. **75**, 3253 (1995).
[13] H. Nha and W. Jhe, Phys. Rev. A (to be published).
[14] J. P. Dowling and J. Gea-Banacloche, Adv. At. Mol. Opt. Phys. **36**, 1 (1996).
[15] S. R. Friberg and R. J. Hawkins, J. Opt. Soc. Am. B **12**, 166 (1995).
[16] L. S. Brown, G. Gabrielse, K. Helmerson, and J. Tan, Phys. Rev. A **32**, 3204 (1985).
[17] A. D. McLachlan, Mol. Phys. **6**, 423 (1963).
[18] E. M. Lifshitz and L. P. Pitaevskii, *Statistical Physics*, 3rd ed. (Pergamon, New York, 1980), Part I, pp. 377–396.
[19] J. D. Jackson, *Classical Electrodynamics*, 2nd ed. (Wiley, New York, 1978), pp. 391–395.
[20] V. Weisskopf, Phys. Rev. **56**, 72 (1939).